









RESEARCH ARTICLE | JULY 10 2023

# High power GaSb-based superluminescent diode with cascade cavity suppression waveguide geometry and ultra-low antireflection coating

Tianfang Wang ; Chengao Yang  ; Yihang Chen; Jianmei Shi ; Hongguang Yu; Xiangbin Su; Yu Zhang; Youwen Zhao ; Cunzhu Tong; Donghai Wu ; Yingqiang Xu ; Haiqiao Ni; Zhichuan Niu 

 Check for updates

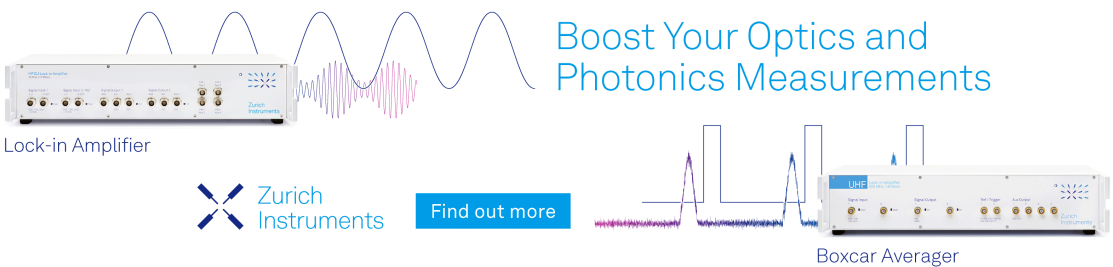
*Appl. Phys. Lett.* 123, 021102 (2023)

<https://doi.org/10.1063/5.0157235>




CrossMark

Boost Your Optics and Photonics Measurements



Lock-in Amplifier

 Zurich Instruments

[Find out more](#)

Boxcar Averager

# High power GaSb-based superluminescent diode with cascade cavity suppression waveguide geometry and ultra-low antireflection coating

Cite as: Appl. Phys. Lett. **123**, 021102 (2023); doi: 10.1063/5.0157235

Submitted: 6 May 2023 · Accepted: 27 June 2023 ·

Published Online: 10 July 2023



View Online



Export Citation



CrossMark

Tianfang Wang,<sup>1,2</sup> Chengao Yang,<sup>1,2,a)</sup> Yihang Chen,<sup>1,2</sup> Jianmei Shi,<sup>1,2</sup> Hongguang Yu,<sup>1,2</sup> Xiangbin Su,<sup>1,2</sup> Yu Zhang,<sup>1,2</sup> Youwen Zhao,<sup>1,2</sup> Cunzhu Tong,<sup>3</sup> Donghai Wu,<sup>1,2</sup> Yingqiang Xu,<sup>1,2,a)</sup> Haiqiao Ni,<sup>1,2</sup> and Zhichuan Niu<sup>1,2,a)</sup>

## AFFILIATIONS

<sup>1</sup>State Key Laboratory for Superlattices and Microstructures, Institute of Semiconductors, Chinese Academy of Sciences, Beijing 100083, China

<sup>2</sup>Center of Materials Science and Optoelectronics Engineering, University of Chinese Academy of Sciences, Beijing 100049, China

<sup>3</sup>Changchun Institute of Optics, Fine Mechanics and Physics, Chinese Academy of Sciences, Changchun 130033, China

<sup>a)</sup>Authors to whom correspondence should be addressed: [yangchengao@semi.ac.cn](mailto:yangchengao@semi.ac.cn); [yingqxu@semi.ac.cn](mailto:yingqxu@semi.ac.cn); and [zcnui@semi.ac.cn](mailto:zcnui@semi.ac.cn)

## ABSTRACT

We report on a GaSb-based superluminescent diode optimized for high-power broadband operation around a wavelength of 2  $\mu\text{m}$ . The high optical power was achieved by the high-quality epitaxial InGaSb/AlGaAsSb type-I quantum well gain material, which was processed into a double-pass amplification configuration. To prevent lasing at high current injection while enabling strong amplified spontaneous emission, a cascade cavity suppression waveguide geometry was designed to connect the vertical rear facet with the reflectivity-suppressed angled front facet. A Ta<sub>2</sub>O<sub>5</sub>/SiO<sub>2</sub> ultra-low antireflection coating with a minimum reflectivity of 0.04% was applied to the front facet for further cavity suppression. This combination allowed the superluminescent diodes to demonstrate a record high single-transverse-mode output power of up to 152 mW under continuous-wave operation at room temperature, with a broad spectral band of 42 nm full width at half maximum. A 25% promotion in optical power has been realized compared to current state-of-the-art devices in this wavelength range, without sacrificing spectral bandwidth. The high-power spectral density characteristics, along with a good beam quality, are well suited for absorption spectroscopy applications and hybrid integration with silicon technology.

Published under an exclusive license by AIP Publishing. <https://doi.org/10.1063/5.0157235>

Superluminescent diodes (SLDs) are edge-emitting semiconductor emitters that operate in the amplified spontaneous emission (ASE) regime. The unique property of SLDs combines the combination of high brightness and good beam directionality of a laser diode (LD), with a broad optical spectrum and low temporal coherence of a light-emitting diode (LED).<sup>1</sup> SLDs operating in the visible and near-infrared telecommunication wavelength region have emerged as ideal light sources for various industrial and commercial applications, such as in fiber-optic gyroscopes, optical coherence tomography (OCT), and wavelength-division multiplexing (WDM) systems.<sup>2–4</sup> Recently, there has been growing interest in trace gas spectroscopy and biomedical imaging applications, which have led to the operational wavelength extension of SLDs to the mid-infrared (mid-IR) region due to the presence of various molecular absorption fingerprints.<sup>5,6</sup>

Mid-IR SLDs are ideal candidates for gas and liquid sensing applications, either as stand-alone broadband light sources or as gain chips in hybrid integrated configurations for tunable laser absorption spectroscopy (TLAS).<sup>7,8</sup> The wider emission spectra of SLDs address the need for the simultaneous monitoring of mixtures of multiple trace gases or complex biomolecules that manifest broad absorption features.<sup>9–11</sup> Their high-power characteristics enable high signal-to-noise ratio detection, especially against the scattering nature of aqueous solutions or human tissues.<sup>12–14</sup> Meanwhile, the good spatial and high beam quality characteristics of SLDs are advantageous for efficient coupling with optical fibers or external cavity elements.<sup>9</sup> The heterogeneous integration of SLDs with silicon photonics integrated circuitry may provide promising prospects for the miniaturization and volume production of optical sensors at a low cost, allowing for various emerging on-chip optical systems.<sup>15,16</sup>

In the 2–3  $\mu\text{m}$  mid-IR wavelength range, the GaSb-based material platform has shown superior optical gain performance, confirmed by the low threshold and high power under room temperature (RT) and continuous-wave (CW) operation of GaSb-based LDs.<sup>17</sup> SLDs generally share similar type-I quantum well (QW) active region epitaxial structures with LDs.<sup>6,18</sup> To acquire superluminescence, cavity feedback must be carefully suppressed for SLDs during manufacturing when the ridge waveguide (RWG), electrical contacts, and facet are defined, based on the concepts of increasing the mirror or waveguide loss. Common approaches, such as angled facets, active or passive absorber sections, and antireflection (AR) coatings, have been effectively demonstrated in previous studies on visible and near-infrared SLDs.<sup>12,19,20</sup> However, for mid-IR SLDs, a longer wavelength inherently requires lower modal reflectivity, thus requiring more delicate longitudinal designs that combine two or more methods, to prevent laser oscillations in the cavity.<sup>18</sup>

In recent years, several groups have reported on attempts and efforts to optimize the cavity design methods, pursuing the optical power and spectral bandwidth enhancement of mid-IR SLDs. Vizbaras *et al.*<sup>9</sup> demonstrated GaSb-based SLD devices that employed an all-curved waveguide geometry and 0.1% low reflectivity AR coating, providing output power up to 40 mW at 2.05  $\mu\text{m}$ , 10 mW at 2.25  $\mu\text{m}$ , and 5 mW at 2.38  $\mu\text{m}$  under CW operation at RT. Wang *et al.*<sup>18</sup> reported on an InP-based SLD that combined a spiral structure with a double-tilted ridge section, achieving a maximum CW output power of 30 mW and spectral full-width at half maximum (FWHM) of 41 nm centered at  $\sim 2.1 \mu\text{m}$ . Zia *et al.*<sup>10</sup> developed a non-index-guided passive absorption section at the output end of the waveguide to further suppress reflections. The researchers combined the absorption sections with a tilted waveguide to realize GaSb-based SLDs with a maximum output power of 60 mW and spectral width of 60 nm FWHM at  $\sim 1.9 \mu\text{m}$ , as well as subsequent results of 3 mW power and 124 nm FWHM in the  $\sim 2.55 \mu\text{m}$  wavelength region in the pulse mode.<sup>11</sup> Furthermore, the researchers developed a double-pass J-shaped waveguide layout, combined with the absorption section and 0.5% AR coating, resulting in a maximum output power of 120 mW at  $\sim 2 \mu\text{m}$  while maintaining a FWHM 40 nm spectral width.<sup>14</sup>

In this work, we develop a high-performance double-pass GaSb-based SLD emitting at  $\sim 2 \mu\text{m}$ , which employed a cascade cavity suppression (CCS) waveguide geometry and high-quality ultra-low antireflection (UAR) coating on the front facet. A high optical power exceeding 150 mW in stable single-transverse-mode emission has been obtained at RT and CW operation, which represents a remarkable improvement compared to the previously reported results in this wavelength region.<sup>14</sup> The power promotion is afforded by the high-quality type-I InGaSb QW epitaxial structures that provide strong material gain and amplified by double-pass configuration. Meanwhile, the optimized waveguide geometry and AR coating provide sufficient strong suppression of the modal reflectivity, even at high current injection levels, allowing for wide and smooth spectral emissions with a bandwidth of 42 nm FWHM at the maximum output power. By varying the current and temperature operating conditions, the 1.92–2.02  $\mu\text{m}$  spectral range can be covered. Furthermore, the transversely confined narrow ridge waveguide (RWG) structure avoids any abrupt changes in the effective refractive index along the entire device, resulting in stable low-astigmatism single-transverse-mode operation, good beam quality with an average  $M^2$  of 1.84, and a small and definite

output port, facilitating the collimation or coupling of the output beam for further utilization.

The epitaxial structure of the investigated SLD was inherited from our previous work on high-power 2  $\mu\text{m}$  GaSb-based RWG LDs grown by molecular beam epitaxy (MBE) on a (100) n-doped GaSb substrate.<sup>21–23</sup> The epilayer stack consisted of two 1.5% compressively strained QWs placed in a separate confinement heterostructure. The two 13 nm  $\text{In}_{0.18}\text{GaSb}$  QWs were separated by a 20 nm lattice-matched  $\text{Al}_{0.25}\text{GaAs}_{0.02}\text{Sb}$  barrier and embedded between two 270 nm  $\text{Al}_{0.25}\text{GaAs}_{0.02}\text{Sb}$  waveguide layers. The undoped waveguide core region was sandwiched between two 2  $\mu\text{m}$   $\text{Al}_{0.5}\text{GaAs}_{0.04}\text{Sb}$  lattice-matched cladding layers. The n-cladding was n-doped to  $1.08 \times 10^{17} \text{cm}^{-3}$ , while the p-cladding layer was p-doped to  $1.4 \times 10^{18} \text{cm}^{-3}$ . The SCH layers were grown on a 360 nm highly n-doped ( $1.3 \times 10^{18} \text{cm}^{-3}$ ) GaSb buffer layer above the GaSb substrate and covered with a 250 nm GaSb cap layer that was highly p-doped ( $5 \times 10^{18} \text{cm}^{-3}$ ) for p-contact. Figure 1(a) presents the schematic epitaxial structure and corresponding photoluminescence spectra peaking at  $\sim 1.93 \mu\text{m}$  measured at RT. The strong intensity indicated the superior quality of the gain material.

In this study, a double-pass waveguide layout was employed to take full advantage of the strong material gain for high-power superluminescence, in which the light propagating toward the rear end would be reflected back and undergo further amplification.<sup>13,14</sup> However, the double effective gain length and strong material gain exposed the SLD to a higher risk of laser oscillation when subjected to small optical feedback. A strong emphasis was placed on the front facet reflectivity suppression.

A common double-pass scheme employs all-curved or J-shaped waveguides to connect the reflected rear facet with an angled front facet to reduce the optical feedback,<sup>9,10</sup> with the facet angle determined by the calculated modal reflectivity resonant dips.<sup>24,25</sup> In this work, we developed a CCS waveguide geometry to improve cavity suppression. As schematically shown in Fig. 1(b), the rear half of the RWG was curved by a large radius of R from the straight rear facet to an angle  $\alpha$  with respect to the cleaved facet for first-stage cavity suppression, while the front half was tilted at a consistent angle  $\alpha$  extending to the angled front facet for second-stage suppression. Transversely confined gain section has been maintained along the whole device to guarantee fundamental transverse mode, facilitating high beam quality and low astigmatism emission. The specific design parameters are shown in Table I.

We studied the design by simulating the mode propagation using finite-difference techniques in the CCS waveguide geometry and compared it to the conventional double-pass J-shape, all-curved, and single-pass all-tilted geometries. The cavity length, facet condition, and other waveguide parameters are kept consistent for comparison. We visualized the process of propagated mode transformation by calculating the mode distribution overlap integral between the modes at various positions along the waveguide and the angled facet mode, inspired by the modal reflectivity calculation based on the overlap integral between the incident and reflected mode fields on the angled facet.<sup>24</sup> The calculation results shown in Fig. 1(c) revealed that the propagated modes in conventional double-pass waveguides gradually transform from the distribution on the straight rear facet to the reflectivity-suppressed mode distribution on an angled facet until propagation reaches the output end. By contrast, the CCS waveguide reaches suppression status at the end of curved first stage, while the tilted second

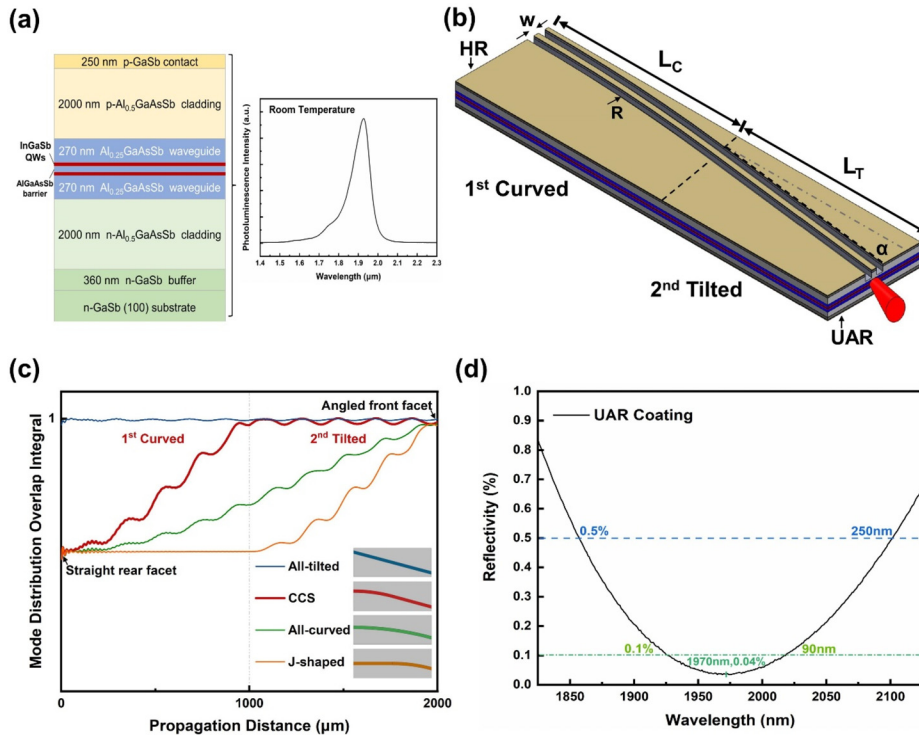


FIG. 1. (a) Schematic epitaxial structure and corresponding photoluminescence spectra measured at room temperature. (b) Schematic drawing of the SLD with a CCS waveguide geometry. (c) Calculated overlap integrals between the propagating modes in the different waveguide designs with the mode distribution on a reflectivity-suppressed 7° angled facet, where the inset in Fig. 1(c) shows the schematic waveguide geometry. (d) Measured reflectivity curve of the UAR coating applied on the front facets.

TABLE I. SLD design parameters.

Label	Description	Value
$L$	Total length of the device	2000 μm
$L_C$	Length of curved RWG	1000 μm
$L_T$	Length of tilted RWG	1000 μm
$R$	Curved radius	8205 μm
$A$	Tilt angle	7°
$W$	Ridge width	5 μm
$n_{eff}$	Effective index of fundamental mode	3.545

stage serves to strengthen the suppression and amplify the gain, similar to the single-pass all-tilted geometry. Additionally, the cascade tilted stage is more in line with the facet angle calculation model,<sup>24,25</sup> leading to better consistency with the expected low reflectivity and higher reliability for cavity suppression, well suited for emitters aimed at high-power superluminescence.

The epi-wafer was processed into SLD devices with CCS waveguide geometry and a cavity length  $L$  of 2 mm. A ridge width  $w$  of 5 μm and a 2.1 μm etch depth were chosen to guarantee the single-transverse-mode operation and strict light guide, according to our previous research on a GaSb-based narrow RWG parameter design.<sup>22</sup> The double-trench RWG structures were defined using contact photolithography and inductively coupled plasma (ICP) etched with BCl<sub>3</sub>/Cl<sub>2</sub>/Ar gas chemistry. The etched RWGs were subsequently isolated by a 250 nm thick SiO<sub>2</sub> layer deposited using plasma-enhanced chemical vapor deposition. A current injection window with a width of 2 μm

was opened at the center of the ridge using negative photoresist lithography and ICP etching, and the Ti/Pt/Au electrode layer was magnetron sputtered on the p-side. To realize high-quality cleaved facets, the wafers were thinned down to ~120 μm. Afterward, the AuGe/Ni/Au electrode layer was sputtered on the substrate side of the wafer and annealed to form the ohmic contact.

To further suppress parasitic lasing and spectral modulation, a high-performance UAR coating consisting of double-layer Ta<sub>2</sub>O<sub>5</sub>/SiO<sub>2</sub> with 191.9/100.7 nm thickness was designed and applied to the angled front facet of the cleaved bars from the processed wafer. The realization of ultra-low reflectivity is mainly attributed to the suitable matching of the refractive index of Ta<sub>2</sub>O<sub>5</sub> for the ~2 μm GaSb-based material. SiO<sub>2</sub> with a gradient lower refractive index serves the purpose of broadening the antireflection band. The ion beam sputtering method was adopted to enhance the applicability and repeatability of the UAR coating, which permitted a sufficiently low average deposition rate of 2 Å/s for accurate thickness control and slight adjustment of the refractive index through pressure control. Figure 1(d) shows the reflectivity spectrum of the UAR coating, measured by a Cary 7000 spectrophotometer. The UAR coating provided a U-shaped antireflection band with a minimum reflectivity as low as 0.04% at a ~1.97 μm center emission wavelength, while maintaining the 90 nm 0.1% reflectivity bandwidth that well covered the device emission spectral range. This was a prominent improvement compared to current state-of-art mid-IR coatings with typical minimum reflectivity of 0.1–0.5%.<sup>8,9,14</sup> In addition, the rear facet was coated with high-reflectivity (>98% from 1.7 to 2.3 μm) coatings for double-pass amplification.

The coated bars were chipped into emitters and were mounted epi-side down on C-mounts. The devices were characterized under

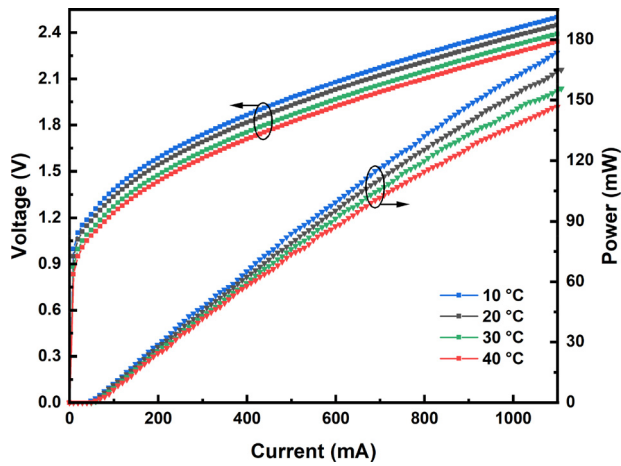


FIG. 2. L–I–V curve for the SLD with a CCS waveguide geometry measured under CW operation at different heat sink temperatures.

CW operation, to measure the light–current–voltage (L–I–V) characteristics, emission spectra, and far-field characteristics. SLDs with all-curved geometry were also fabricated in the same bar with the CCS devices, for comparison.

Figure 2 shows the P–I–V characteristics of the CCS SLDs measured at different temperatures. The output power increased super-linearly up to a few milliwatts, indicating amplified spontaneous emission and then sub-linearly due to gain saturation and heat accumulation. The SLDs achieved a maximum CW output power of 152 mW under 1 A at 20 °C, resulting in 25% promotion compared to the best power results of GaSb SLDs in this wavelength region.<sup>14</sup> When the operating temperature decreased to 10 °C, the maximum output power reached 160 mW at 1 A, and the output power was still 137 mW when the operating temperature was increased to 40 °C. We attributed the power scaling to the superior quality of our epitaxially grown layers, and thus, higher material gain. The CCS SLD devices with relatively higher curving losses exhibited less than 10 mW disadvantageous power results at 1 A injection current compared to the J-shaped and all-curved devices, due to a relatively longer amplification length. The maximum CW output power of these devices was limited

by the catastrophic optical damage (COD) that typically occurs in the 1.1–1.4 A current range, originating from the heavy optical density load on the very small emitting facet area. Facet passivation is a potential method to increase the COD threshold for further promotion of the injection level and output power of the CCS SLDs. Relevant investigation will be performed in the future.

The spectral emission for the CCS SLDs under different operating currents and temperatures are shown in Fig. 3. The fairly broad spectral width of 42 nm FWHM at maximum output power under 1 A and 20 °C was equivalent to the previous results of GaSb SLDs with double-pass gain geometry, providing clear evidence of operation in the superluminescent regime. A smooth spectrum with no lasing sign and spectral modulation revealed the low modal reflectivity. By contrast, relatively prominent laser fringes and spectral modulation of the spontaneous emission were observed in the emission spectra of the J-shaped and all-curved SLDs under the same working conditions of 1 A and 20 °C, as shown in the inset of Fig. 3(a). We attributed the improvement mainly to the optimal CCS cavity design. As shown in Fig. 3(a), spectral broadening from 33 to 42 nm FWHM was observed with the injection current increasing from 0.6 to 1.0 A, which could be attributed to the rapid increase in material gain bandwidth. The effect of temperature on the emission spectra is shown in Fig. 3(b). A red shift of about 1.4 nm/°C in the spectral peak was observed oriented from the material bandgap shrinkage with temperature. The injection level along with the working temperature could be used as an opportunity to tune the SLD spectrum from  $\sim 1.95$  to  $\sim 2$   $\mu\text{m}$ , expanding the application feasibility of the SLD devices.

The lateral far-field characteristic of the CCS SLDs measured at the maximum output power is shown in Fig. 4, indicating the corresponding 21° FWHM divergence angles. A shift of 25.6° in the beam exit angle of the lateral direction was due to the tilted RWG, which could be determined by Snell's law. The beam width under the second-order moment ( $D4\sigma$ ) definition at different positions was measured along the lateral and vertical directions with a scanning-slit beam profiler, as shown in the inset of Fig. 4. The  $M^2$  factors of  $1.94 \times 1.73$  (vertical  $\times$  lateral) were derived from the hyperbola fit. The far-field intensity pattern of the collimated emission beam from the SLD is also shown as an inset. The Gaussian shape far-field beam profiles without any side lobes at a high injection level of 1 A and  $M^2$  factor below 2 reveals the stable single-transverse-mode operation

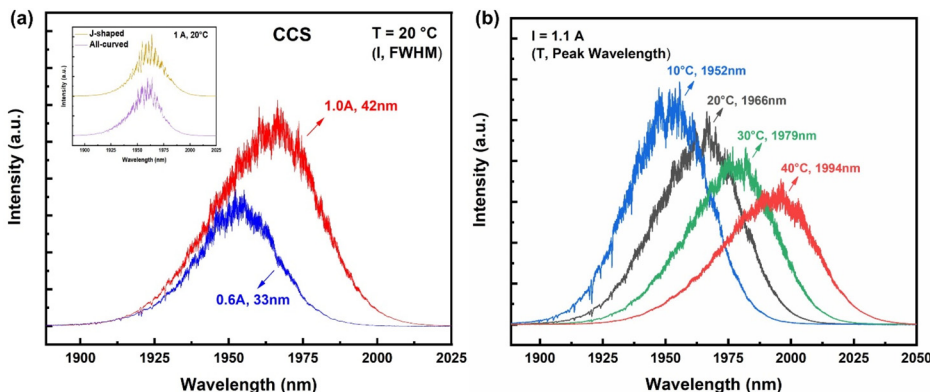
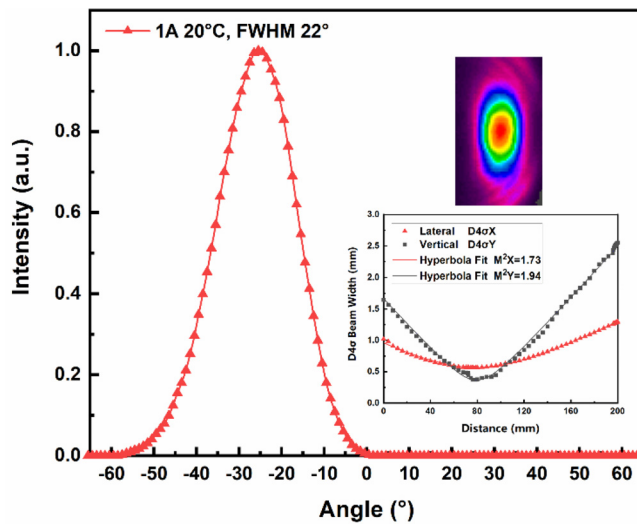


FIG. 3. The emission spectra of the SLD with a CCS waveguide geometry measured under CW injection at (a) different currents and constant 20 °C heat sink temperature and (b) different temperatures and constant 1.1 A current, where the inset in Fig. 3(a) represents the emission spectra of the SLDs with J-shaped and all-curved geometries at 1 A and 20 °C, and the arrows indicate the corresponding operating conditions and (a) full-width at half maximum (FWHM) or (b) peak wavelength.



**FIG. 4.** Slow axis far-field profile of the CCS SLD measured at 1 A and 20 °C, where the inset shows the D4 $\sigma$  beam width variations and far-field image pattern of the collimated beam from the SLD.

and good beam quality of the CCS SLDs. This beam performance combined with the clear RWG output ports, guaranteed the ability of these devices to be conveniently and efficiently coupled into a single-mode optical fiber or a silicon photonics integrated circuit.

In conclusion, we demonstrated electrically pumped CW high-power, single-transverse-mode SLDs operated near 2  $\mu\text{m}$ . The SLD device provided a recorded high output power of 152 mW, with simultaneously broad and smooth spectra of 42 nm FWHM width at an injection current of 1 A and 20 °C. These characteristics are attributed to the high material gain provided by our high-quality type-I InGaSb/AlGaAsSb QW active region epitaxy, along with the implementation of a CCS double-pass waveguide geometry and ultra-low reflectivity antireflection coating. Compact and power-efficient SLD devices with this level of high power, broad emission spectra, and excellent beam quality can be an ideal laser source for various hybrid integration and spectroscopy applications.

This research was funded by the National Natural Science Foundation of China (Grant No. 62204238); the project of “Announce the list and take charge” of the major special plan of science and technology in Shanxi Province (Grant No. 202201030201009); the Chinese Academy of Sciences and Changchun City Science and Technology Innovation Cooperation Project (GrantNo. 21SH06); the Jincheng Key Research and Development Project (Grant No. 20210209); the Key R&D Program of Shanxi Province (Grant No. 202102030201004); and the Innovation Program for Quantum Science and Technology (Award/Contract No. 2021ZD0300801).

## AUTHOR DECLARATIONS

### Conflict of Interest

The authors have no conflicts to disclose.

## Author Contributions

**Tianfang Wang:** Conceptualization (equal); Investigation (lead); Methodology (equal); Visualization (equal); Writing – original draft (lead); Writing – review & editing (equal). **Donghai Wu:** Writing – review & editing (equal). **Yingqiang Xu:** Funding acquisition (equal); Writing – review & editing (equal). **Haiqiao Ni:** Project administration (supporting); Supervision (supporting). **Zhichuan Niu:** Funding acquisition (equal); Project administration (equal); Supervision (equal). **ChengAo Yang:** Conceptualization (equal); Funding acquisition (equal); Writing – review & editing (equal). **Yihang Chen:** Resources (equal). **Jianmei Shi:** Visualization (equal). **Hongguang Yu:** Resources (equal). **Xiangbin Su:** Methodology (equal). **Yu Zhang:** Resources (equal). **Youwen Zhao:** Writing – review & editing (equal). **Cunzhu Tong:** Writing – review & editing (equal).

## DATA AVAILABILITY

The data that support the findings of this study are available from the corresponding authors upon reasonable request.

## REFERENCES

- C. C. Hou, H. M. Chen, J. C. Zhang, N. Zhuo, Y. Q. Huang, R. A. Hogg, D. T. Childs, J. Q. Ning, Z. G. Wang, F. Q. Liu *et al.*, *Light: Sci. Appl.* **7**, 17170 (2018).
- W. Burns and R. Moeller, *J. Lightwave Technol.* **2**(4), 430–435 (1984).
- D. Huang, E. A. Swanson, C. P. Lin, J. S. Schuman, W. G. Stinson, W. Chang, M. R. Hee, T. Flotte, K. Gregory, C. A. Puliafito *et al.*, *Science* **254**(5035), 1178–1181 (1991).
- S. J. Russell, K. R. C. Brady, and J. P. Dakin, *J. Lightwave Technol.* **19**(2), 205–213 (2001).
- C. Grasse, T. Gruendl, S. Sprengel, P. Wiecha, K. Vizbaras, R. Meyer, and M.-C. Amann, *J. Cryst. Growth* **370**, 240–243 (2013).
- M. B. Wootten, J. Tan, Y. J. Chien, J. T. Olesberg, and J. P. Prineas, *Semicond. Sci. Technol.* **29**(11), 115014 (2014).
- S. P. Ojanen, J. Viheriälä, M. Cherchi, N. Zia, E. Koivusalo, P. Karioja, and M. Guina, *Appl. Phys. Lett.* **116**(8), 081105 (2020).
- T. F. Wang, C. G. Yang, Y. Zhang, Y. H. Chen, J. M. Shang, Y. Zhang, Y. Q. Xu, and Z. C. Niu, *Opt. Express* **29**(21), 33864–33873 (2021).
- K. Vizbaras, E. Dvinelis, I. Šimonytė, A. Trinkūnas, M. Greibus, R. Songaila, T. Žukauskas, M. Kaušylas, and A. Vizbaras, *Appl. Phys. Lett.* **107**(1), 011103 (2015).
- N. Zia, J. Viheriälä, R. Koskinen, A. Aho, S. Suomalainen, and M. Guina, *Appl. Phys. Lett.* **109**(23), 231102 (2016).
- N. Zia, J. Viheriälä, E. Koivusalo, H. Virtanen, A. Aho, S. Suomalainen, and M. Guina, *Appl. Phys. Lett.* **112**(5), 051106 (2018).
- G. R. Goldberg, D. H. Kim, R. J. E. Taylor, D. T. D. Childs, P. Ivanov, N. Ozaki, K. L. Kennedy, K. M. Groom, Y. Harada, and R. A. Hogg, *Appl. Phys. Lett.* **117**(6), 061106 (2020).
- A. Kafar, S. Stańczyk, P. Wiśniewski, T. Oto, I. Makarowa, G. Targowski, T. Suski, and P. Perlin, *Phys. Status Solidi A* **212**(5), 997–1004 (2015).
- N. Zia, J. Viheriälä, E. Koivusalo, and M. Guina, *Appl. Phys. Lett.* **115**(23), 231106 (2019).
- R. J. Wang, S. Sprengel, A. Vasiliev, G. Boehm, J. Van Campenhout, G. Lepage, P. Verheyen, R. Baets, M.-C. Amann, and G. Roelkens, *Photonics Res.* **6**(9), 858 (2018).
- R. J. Wang, A. Malik, I. Šimonytė, A. Vizbaras, K. Vizbaras, and G. Roelkens, *Opt. Express* **24**(25), 28977 (2016).
- M. Rattunde, J. Schmitz, G. Kaufel, M. Kelemen, J. Weber, and J. Wagner, *Appl. Phys. Lett.* **88**(8), 081115 (2006).
- D. B. Wang, J. C. Zhang, C. C. Hou, Y. Zhao, F. M. Cheng, X. F. Jia, S. Q. Zhai, N. Zhuo, J. Q. Liu, F. Q. Liu *et al.*, *Appl. Phys. Lett.* **113**(16), 161107 (2018).

- <sup>19</sup>A. T. Aho, J. Viheriälä, H. Virtanen, N. Zia, R. Isoaho, and M. Guina, *Appl. Phys. Lett.* **115**(8), 081104 (2019).
- <sup>20</sup>A. Kafar, S. Stańczyk, S. Grzanka, R. Czernecki, M. Leszczyński, T. Suski, and P. Perlin, *J. Appl. Phys.* **111**(8), 083106 (2012).
- <sup>21</sup>S. W. Xie, Y. Zhang, C. A. Yang, S. S. Huang, Y. Yuan, Y. Zhang, J. M. Shang, F. H. Shao, Y. Q. Xu, H. Q. Ni *et al.*, *Chin. Phys. B* **28**(1), 014208 (2019).
- <sup>22</sup>T. F. Wang, C. G. Yang, Y. H. Chen, J. M. Shi, H. G. Yu, X. B. Su, Y. Zhang, Y. Q. Xu, and Z. C. Niu, *Nanoscale Res. Lett.* **17**(1), 116 (2022).
- <sup>23</sup>C. A. Yang, S. W. Xie, Y. Zhang, J. M. Shang, S. S. Huang, Y. Yuan, F. H. Shao, Y. Zhang, Y. Q. Xu, and Z. C. Niu, *Appl. Phys. Lett.* **114**(2), 021102 (2019).
- <sup>24</sup>G. A. Alphonse and M. Toda, *J. Lightwave Technol.* **10**(2), 215–219 (1992).
- <sup>25</sup>D. Marcuse, *J. Lightwave Technol.* **7**(2), 336–339 (1989).